

Mechanisms that increase the growth efficiency of diatoms in low light

Nerissa L. Fisher¹ · Kimberly H. Halsey²

Received: 21 January 2016 / Accepted: 7 June 2016 / Published online: 16 June 2016
© Springer Science+Business Media Dordrecht 2016

Abstract Photoacclimation was studied in *Thalassiosira pseudonana* to help understand mechanisms underlying the success of diatoms in low-light environments, such as coastal and deep mixing ecosystems. Light harvesting and other cell characteristics were combined with oxygen and carbon production measurements to assess the water-splitting reaction at PSII (GPP_{O_2}) and intermediate steps leading to net carbon production (NPP_C). These measurements revealed that *T. pseudonana* is remarkably efficient at converting harvested light energy into biomass, with at least 57 % of GPP_{O_2} retained as NPP_C across all light-limited growth rates examined. Evidence for upregulation of ATP generation pathways that circumvent carbon fixation indicated that high growth efficiency at low light levels was at least partly due to increases in the efficiency of ATP production. Growth rate-dependent demands for ATP and NADPH were reflected in carbon composition and in unexpected shifts in the light-limited slope (α) of photosynthesis–irradiance relationships generated from chlorophyll-specific ^{14}C -uptake. Overall, these results suggest that pathway gating of carbon and energy flow depends on light availability and is a key factor promoting the efficiency of diatom growth at low light intensities.

Keywords Photoacclimation · Photosynthetic energy allocation · Photosynthesis · Phytoplankton · Diatoms · Light limitation · Alternative pathways

Introduction

Diatoms are major contributors to oceanic primary production (Field et al. 1998; Smetacek 1999). Their ubiquity and dominance in coastal and upwelling regions indicate that diatoms possess unique adaptive strategies (Crombet et al. 2011; Kooistra and Medlin 2007; Margalef 1978). Indeed, it has been suggested that diatoms are unusual in their growth efficiency at low light intensities (Furnas 1990), but biochemical and physiological mechanisms that support this idea have not been identified (Bowler et al. 2010).

Photoacclimation involves generally predictable changes in pigment concentration and photosynthetic rates that function to balance light absorption with downstream carbon metabolism (Behrenfeld et al. 2008; Geider 1987; Vandenhecke et al. 2015). By definition, cells that are photoacclimated to their light environment have achieved balanced growth because their physiology has adjusted to reach equilibrium (MacIntyre and Cullen 2005). Studies on photoacclimation lead to quantitative descriptions of growth for estimates and predictions of the marine carbon cycle (Flynn 2001; Geider et al. 1998, 2009) and can reveal new metabolic mechanisms that function to optimize phytoplankton growth (Six et al. 2008; Su et al. 2012; Wagner et al. 2006).

Following light absorption, photosynthesis is initiated by the light-dependent excitation of an electron originating from the splitting of H_2O . These high-energy electrons are passed from PSII through an electron transport chain terminating at $NADP^+$ to form NADPH. As with respiratory electron transport, a proton motive force is created in the process of photosynthetic electron transport and used to generate ATP. NADPH and ATP fuel CO_2 fixation through the Calvin Benson cycle. However, the stoichiometry of ATP:NADPH produced through photosynthesis may not perfectly match the requirements for CO_2 fixation and

✉ Kimberly H. Halsey
halseyk@science.oregonstate.edu

¹ Department of Botany and Plant Pathology, Oregon State University, 2082 Cordley Hall, Corvallis, OR 97331, USA

² Department of Microbiology, Oregon State University, 226 Nash Hall, Corvallis, OR 97331, USA

other metabolic demands that vary depending on environmental conditions. Additional ATP can be generated through alternative pathways including light-dependent respiration (LDR) and cyclic PSI electron transport (Allen 2003; Asada 1999). LDR pathways include midstream oxidase activity and the Mehler reaction which enhance the proton motive force across the thylakoid membrane. In addition, the malate valve transfers reducing equivalents from the plastid directly to the mitochondrial respiratory electron transport chain. These alternative pathways function only in the light, circumvent carbon fixation, and can significantly influence the efficiency of light energy conversion to biomass (Halsey and Jones 2015; Kunath et al. 2012).

Prihoda suggested that inter-organelle transfers of carbon and electrons might be a mechanism that diatoms use to fine-tune their energy balance (ATP:NADPH) (Prihoda et al. 2012). Features of diatoms that support this idea include (1) reports of high growth efficiencies in diatoms (Furnas 1990; Wagner et al. 2006), (2) chloroplasts and mitochondria that are tightly appressed, in contrast to many other microalgae (Prihoda et al. 2012), (3) some carbon metabolism enzymes that are located in the cytosol, as opposed to the plastids (Wilhelm et al. 2006), (4) a subset of these enzymes participate in interconnecting primary carbon pathways: the glycolytic, pentose phosphate, and Calvin Benson pathways, (5) evidence for a full glycolytic pathway within diatom mitochondria (Smith et al. 2012), and (6) sensitivity of photosynthesis to disruption of mitochondrial terminal oxidase activity (Bailleul et al. 2015). These unique features of diatom carbon metabolism are postulated to facilitate flexible and highly responsive intracellular control of carbon and energy flux (Singh et al. 2015). While these observations and the ecology of diatoms have been linked by conjecture, as yet, no evidence for mechanisms underlying high growth efficiency of diatoms at low light, or the implementation of efficient pathways at low light, has been reported.

One reason that pathways altering growth efficiency are elusive to measure is that photosynthetic cells typically employ many other controls that are responsive to environmental conditions and alter photosynthetic properties. Changes in cellular pigment and carbon content and their effects on fundamental measurements of photosynthesis during light-limited growth are well described (MacIntyre et al. 2002; Laws and Bannister 1980). However, a more complete accounting of the total energy harvested through photosynthesis and how that energy is used to fuel growth processes across a wide range of growth-limiting irradiances can help understand variability in commonly collected data such as photosynthesis–irradiance (PE) relationships (Halsey et al. 2010; Behrenfeld et al. 2008), the caloric content of biomass (Halsey et al. 2011; Jakob

et al. 2007), and energy use efficiencies (Halsey and Jones 2015).

In this study we simultaneously quantified many properties of photosynthetic energy use in light-limited cultures of the model diatom, *Thalassiosira pseudonana*, which enabled an accurate accounting of the distribution of energy through interconnected metabolic pathways. The results confirmed that *T. pseudonana* is highly efficient at converting harvested light energy to biomass and provided direct evidence for mechanisms that can shift the flow of carbon or electrons to shorter, more efficient pathways at low light levels. Some of these metabolic shifts may be specific to diatoms, while others (especially growth rate-dependent carbon metabolism) appear to be shared by many microalgae.

Materials and methods

Culture conditions and characteristics

A complete listing of abbreviations used throughout this manuscript is provided in Table 1. For brevity, and by convention, production measures with a superscripted ‘b’ indicate values normalized to chlorophyll_a concentration (Chl_a), and a superscripted ‘C’ indicates production values normalized to carbon content (Table 1).

Thalassiosira pseudonana (Hustedt) Hasle et Heimdal CCMP 1355 was grown in 300 ml continuous culturing systems at 18 °C using f/2 + Si medium (Guillard 1975) supplemented with Na₂SeO₃ at 0.17 μM concentration. Nitrate and phosphate concentrations in the media reservoir were 250 and 50 μM, respectively (Laws and Bannister 1980). Data were collected from at least three independent continuous cultures grown at a constant light intensity of 200, 60, or 5 μmol photons m⁻² s⁻¹. Cultures were first grown under each light intensity to determine the light-dependent growth rates. For continuous cultures, growth rates were maintained by setting peristaltic pumps to administer media at flow rates according to the equation

$$\mu = \frac{D}{V},$$

where μ is the specific growth rate (day⁻¹), D is flow rate (ml day⁻¹), and V is culture volume (300 ml). Light was supplied by cool-white fluorescent tubes and intensities were measured with a quantum meter (Biospherical Instruments QSL-100) with a 4 π spherical quantum sensor. Cultures were continuously bubbled to keep cells in suspension, exposed to the same average light intensity, and to ensure that CO₂ was not limiting. All cultures were acclimated to their growth irradiances for at least 10 generations. Steady-state growth was verified by the measurement

Table 1 Abbreviations and definitions of properties measured in this study

Symbol	Definition	Units
μ	Specific growth rate	d^{-1}
Chl	Chlorophyll <i>a</i>	
\bar{a}^b	Chl-normalized, spectrally averaged absorption coefficient	$\text{m}^2 (\text{mg Chl})^{-1}$
F_V/F_M	Variable fluorescence	Dimensionless
σ_{PSII}	Functional absorption cross section of PSII	$\text{m}^2 \text{g Chl}^{-1}$
α^b	Light-limited slope of the Chl-normalized PE curve	$\mu\text{mol O}_2 \text{ or C m}^2 \text{ s} (\text{mg Chl h } \mu\text{mol photons})^{-1}$
α^c	Light-limited slope of the carbon-normalized PE curve	$\text{mol O}_2 \text{ or C m}^2 \text{ s} (\text{mol C h } \mu\text{mol photons})^{-1}$
ϕ_m	Maximum quantum yield of photosynthesis	$\text{mol O}_2 \text{ or C} (\text{mol photons})^{-1}$
P_{max}^b	Chl-normalized light saturated rate of photosynthesis	$\mu\text{mol O}_2 \text{ or C} (\text{mg Chl h})^{-1}$
P_{lg}^b	Chl-normalized rate of photosynthesis at the growth irradiance	$\mu\text{mol O}_2 \text{ or C} (\text{mg Chl h})^{-1}$
P_{lg}^c	C-normalized light saturated rate of photosynthesis	$\text{mol O}_2 (\text{mol C d})^{-1} \text{ or } \text{d}^{-1}$
E_k	Light-saturation index	$\mu\text{mol photons m}^{-2} \text{ s}^{-1}$
GPP_{O_2}	Gross O ₂ production	$\mu\text{mol O}_2 \text{ h}^{-1}$
$\text{GPP}_{\text{O}_2}^b$	Chl-normalized gross O ₂ production	$\mu\text{mol O}_2 (\text{mg Chl h})^{-1}$
$\text{GPP}_{\text{O}_2}^c$	C-normalized gross O ₂ production	$\text{mol O}_2 (\text{mol C d})^{-1}$
GP_C	Gross carbon production	$\mu\text{mol C h}^{-1}$
LDR^b	Chl-normalized light-dependent respiration	$\mu\text{mol O}_2 (\text{mg Chl h})^{-1}$
$\text{NP}_{\text{O}_2/\text{C}}^b$	Chl-normalized net O ₂ production	$\mu\text{mol C} (\text{mg Chl h})^{-1}$
$\text{NP}_{\text{O}_2/\text{C}}^c$	C-normalized net O ₂ production	d^{-1}
NPP_C^b	Chl-normalized net carbon production	$\mu\text{mol C} (\text{mg Chl h})^{-1}$
DR	Dark respiration	$\mu\text{mol C} (\text{mg Chl h})^{-1}$
MMR	Maintenance mitochondrial respiration	$\mu\text{mol C} (\text{mg Chl h})^{-1}$
$\text{C}_r:\text{C}_o$	Biochemical reduction state of cell carbon	Dimensionless

of cell concentrations that varied <5 % over 3 days before performing experiments. Cell concentration, diameter, and volume were measured using a Multisizer 3 Coulter Counter equipped with a 100- μm aperture tube (Beckman Coulter; Miami, FL).

Chl*a* was determined in triplicate by filtering 4–6 ml culture onto a 25 mm glass fiber filter (Whatman GF/F) that was extracted overnight at -20°C in 90 % acetone. Absorptivity was measured by spectrophotometry and Chl*a* was quantified according to the equation from Ritchie (2006). The Chl*a*-specific spectrally averaged absorption coefficient (\bar{a}^b) was measured by the filter pad method with corresponding path length corrections (Mitchell et al. 2003). There were no significant differences in \bar{a}^b calculated using the spectral distributions of different light sources (cool-white fluorescent tubes vs. Eiko 2450 ELH 300 W 120 V halogen bulbs (Shawnee, KS) used in collection of photosynthetic irradiance (PE) data (see below)).

Cellular carbon and nitrogen were measured using 2, 3, and 4 ml culture samples, filtered onto precombusted GF/F filters. Culture filtrate (4 ml) was also analyzed for background subtraction. Samples were measured on an Exeter Analytical EA1 elemental analyzer (Coventry, England).

NPP_C was calculated as the product of specific growth rate (μ) and cellular carbon values according to the equation

$$\text{NPP}_C = \mu C.$$

Photosynthesis–irradiance (PE) determinations

PE relationships were determined by short-term exposures of culture samples to ranges of light intensities while measuring O₂ production or ¹⁴C-uptake. We used membrane inlet mass spectrometry (MIMS) and the ¹⁸O₂:¹⁶O₂ method to simultaneously quantify gross O₂ production (GPP_{O_2}), net O₂ production, and LDR (Halsey et al. 2010, 2013). A 150–200 ml culture sample was concentrated to approximately 5 ml using a 2- μm polycarbonate membrane filter and a 47-mm GF/F backing filter. During concentration, cells were kept in suspension to further minimize cell stress. The concentrated sample and the ¹⁸O₂ tracer (final concentration of 40–70 μM) were added to a 5-ml Dubinsky chamber (Dubinsky et al. 1987). The sample was continuously stirred at ~ 8 Hz using a magnetic stir bar and incubated at 20°C . The chamber was mounted to the membrane inlet system and attached to a Prisma QMS-200 (Pfeiffer) quadrupole mass spectrometer with a closed

ion source and electron multiplier detector for recording mass/charge (m/z) ratios of 32 ($^{16}\text{O}_2$), 36 ($^{18}\text{O}_2$), and 40 (Ar). All sample incubations began with a 5-min dark period to confirm highly similar rates of $^{16}\text{O}_2$ and $^{18}\text{O}_2$ consumption in the dark (DR, dark respiration). Concentrated cell suspensions were exposed to set ranges of nine target light levels (4 min per light level) that corresponded with culture growth intensities. For cultures grown at $5 \mu\text{mol photons m}^{-2} \text{ s}^{-1}$, suspensions were exposed to light intensities ranging from approximately 3–200 $\mu\text{mol photons m}^{-2} \text{ s}^{-1}$. For cultures grown at 60 $\mu\text{mol photons m}^{-2} \text{ s}^{-1}$, light exposures ranged from 5 to 650 $\mu\text{mol photons m}^{-2} \text{ s}^{-1}$, and for cultures grown at 200 $\mu\text{mol photons m}^{-2} \text{ s}^{-1}$, light exposures ranged from approximately 12 to 1500 $\mu\text{mol photons m}^{-2} \text{ s}^{-1}$. PE curves for GPP_{O_2} and $\text{NP}_{\text{O}_2/\text{C}}$ were modeled using a hyperbolic tangent (Smith and Platt 1984). At the completion of each experiment, the concentrated culture sample was retained for measurement of Chl *a*. Net O_2 production was determined from $^{16}\text{O}_2$ signals. GPP_{O_2} production was determined from $^{16}\text{O}_2$ and $^{18}\text{O}_2$ signals in the light. LDR was determined by difference in $^{18}\text{O}_2$ signals in the light and dark. Rates of oxygen production and consumption were calculated by dividing the observed rates by the fraction of $^{16}\text{O}_2$ or $^{18}\text{O}_2$ present during each light exposure to account for changes in isotope dilution throughout the experiment.

To account for variations in the cell densities and Chl *a* of concentrated culture suspensions added to the Dubinsky chamber, Chl *a* versus light intensity relationships were determined for cells grown at each of the three growth irradiances. First, cultures were concentrated by filtration to cell concentrations exceeding that used in MIMS experiments and transferred to the chamber. The light level associated with each neutral density filter was measured using a 4π sensor inserted into the chamber. The concentrated cell suspension was subsequently diluted and light and Chl *a* levels re-measured. This process was repeated four times and resulted in a set of equations for each neutral density filter and cells grown at the three different irradiances. These equations were used to calculate the actual light exposures used in each MIMS experiment.

For short-term (20 min) ^{14}C -uptake experiments, 5 ml culture sample was diluted with 8 ml f/2 + Si media and spiked with 5 $\mu\text{Ci NaH}^{14}\text{CO}_3$. The ^{14}C -spiked sample was aliquoted to 14 six ml scintillation vials and exposed to an appropriate range of 10 light intensities (0–500 $\mu\text{mol photons m}^{-2} \text{ s}^{-1}$ for cells grown at the lowest light intensity, 0–1500 $\mu\text{mol photons m}^{-2} \text{ s}^{-1}$ for cells grown at the higher light intensities) from two tungsten projector bulbs using a photosynthetron (CHPT Mfg Inc; Georgetown, DE) for 20 min at 20 °C. Light intensities were measured using a 4π PAR sensor. After incubation, all

samples were acidified with 10 % HCl and allowed to degas overnight. To measure total activity of the radioactive label added to the samples, two 50 μl subsamples of the inoculated sample were added to 50 μl phenethylamine and 900 μl H_2O .

Other photosynthesis measurements and calculations

To quantify dissolved organic carbon excretion rates (DO^{14}C), a 30.2 ml culture sample was inoculated with 10 $\mu\text{Ci NaH}^{14}\text{CO}_3$, and 5 ml aliquoted into each of six vials. Three of the vials were wrapped with foil for “dark” controls, and three were incubated at the growth irradiance at 18 °C for 24 h. Two subsamples were collected and measured for total activity of radioactive label. After 24 h, samples were gently filtered through GF/F filters. The filtrate was acidified with 10 % HCl and degassed overnight. Total activity was determined for all samples as described above.

Photosynthetic energy (NADPH) used directly for NO_3^- and SO_4^{2-} reduction (DU_{NS}) was accounted for by first using cellular N from the CHN analysis and an assumed N:S ratio of 16:1.3 (Ho et al. 2003) according to the equation

$$\text{DU}_{\text{NS}} = [(2\mu(N + S)) + \text{GPP}_{\text{O}_2}](\text{GPP}_{\text{O}_2})^{-1},$$

where 2 is a factor derived from the eight electrons required to reduce NO_3^- or SO_4^{2-} and four electrons released per O_2 molecule formed from the water-splitting reaction at PSII. Resultant DU_{NS} values were used to calculate gross carbon fixation (GP_{C}) with the equation

$$\text{GP}_{\text{C}} = (\text{GP}_{\text{O}_2} - \text{LDR})(\text{DU}_{\text{NS}})^{-1}.$$

The amount of energy used for NO_3^- and SO_4^{2-} reduction is thus determined by

$$(\text{GP}_{\text{O}_2} - \text{LDR}) - \text{GP}_{\text{C}}.$$

DU_{NS} values were also used to convert net O_2 production to carbon units ($\text{NP}_{\text{O}_2/\text{C}}$) to allow direct comparisons between GP_{C} , measures of $\text{NP}_{\text{O}_2/\text{C}}$, and NPP_{C} following the equation

$$\text{NP}_{\text{O}_2/\text{C}} = (\text{net } \text{O}_2 \text{ production})(\text{DU}_{\text{NS}})^{-1}.$$

Maintenance mitochondrial respiration (MMR) is organic carbon respired to CO_2 when incubated at the growth intensity and was calculated as

$$\text{MMR} = \text{GP}_{\text{C}} - \text{NP}_{\text{O}_2/\text{C}}.$$

Variable fluorescence [$F_{\text{V}}/F_{\text{M}} = (F_{\text{M}} - F_{\text{O}})/F_{\text{M}}$] was determined using fast repetition rate fluorometry [FRRf; (Kolber et al. 1998)] after samples were dark incubated for

5 min prior to initial fluorescence (F_O) and maximal fluorescence (F_M) measurements. F_O is Chla fluorescence when functional PSII reaction centers are fully oxidized, and F_M is the Chla fluorescence when the reaction centers are reduced. Sigma (σ_{PSII}) was also recorded to monitor the functional absorption cross section of PSII.

Biochemical fractionation

^{14}C -pulse labeling experiments were done to measure incorporation of labeled carbon into different macromolecular pools. Culture samples (60.2 ml) were spiked with 15 μCi $\text{NaH}^{14}\text{CO}_3$, aliquoted into three 20 ml vials, and incubated at the growth irradiance at 18 °C for 20 min. Cells were filtered onto GF/F filters, rinsed three times with 10 ml *f/2* + Si media, and frozen at –20 °C for later extraction, fractionation, and quantification (Smith and Geider 1985). Two activity subsamples were collected and measured using the procedure described above. Filters were dried under the flow hood overnight then 1.5 ml 2:1 (v/v) chloroform:methanol added and samples extracted at –20 °C for 12–24 h. The extracted sample was filtered through a GF/F filter that was rinsed twice with 2:1 chloroform:methanol. 1 ml dH_2O was added to the filtrate before centrifuging at 1400 rpm (Eppendorf 5418, USA Scientific) for 5 min. The top layer containing the lipid fraction was transferred to a scintillation vial. The aqueous/alcohol layer containing LMW metabolites was transferred to a second scintillation vial. The two filters were placed into a scintillation vial and extracted in 2 ml 5 % trichloroacetic acid (TCA) at 80 °C for 60 min. This hot TCA extract was filtered through another GF/F and rinsed 2 \times with 2 ml 5 % TCA leaving 3 filters in one vial containing the protein fraction. The filtrate contained the carbohydrate and some nucleic acids and was evaporated to about 2 ml.

Cellular protein and carbohydrate assays supplemented 20 min pulse-label experiments. For protein assays, 8–10 ml culture was filtered in duplicate on a 25-mm Durapore PVDF membrane filter (Merck Millipore, Tullagreen, Ireland) and then stored at –80 °C. Upon thaw, 0.6 ml 0.2 μm filtered artificial seawater and 0.6 ml 0.2 M NaOH were added to each filter. Samples were vortexed, sonicated for 15 min, and heated at 100 °C for 20 min. Following centrifugation at 17,000 $\times g$, 0.8 ml supernatant was collected, and protein content was measured spectrophotometrically using a Thermo Scientific Pierce Micro BCA Protein Assay Kit (Eugene, OR, USA) with bovine serum albumin as standards.

For carbohydrate determination, 20–30 ml culture was filtered in duplicate onto a combusted GF/C filter and stored at –20 °C for later extraction. Filters were thawed and then incubated in 5 ml 0.05 M H_2SO_4 for 20 min at 60 °C. Extracts were filtered onto a GF/C to collect cellular

β -1,3-glucan and stored at 4 °C (Granum et al. 2002). The original filter containing cell wall polysaccharide was washed with dH_2O and then dried at 60 °C overnight. After drying, the polysaccharide was hydrolyzed using 0.5 ml 80 % H_2SO_4 at 0–4 °C for 20 h, 6 ml ice cold H_2O was added, and the solution was filtered onto another GF/C to collect cell wall hydrolyzate. 0.5 ml 3 % aqueous phenol and 5 ml concentrated sulfuric acid were added and allowed to stand for 30 min before measuring absorption at 485 nm. Standards were measured using analytical grade D-(+)-glucose (Supelco, Bellefonte, PA, USA). Across all growth rates, structural cell wall carbohydrates were less than 5 % of total carbohydrate. For comparison to pulse-labeled carbohydrate measurements, cell wall and cellular β -1,3-glucan fractions were combined to yield total carbohydrate fractions.

Results

Light-limited continuous cultures of *T. pseudonana* were grown at 5, 60, and 200 $\mu\text{mol photons m}^{-2} \text{s}^{-1}$ yielding specific growth rates of 0.20, 0.85, and 1.54 d^{-1} , respectively. These growth rates achieved using constant light conditions (Table 1) were remarkably similar to growth rates achieved for *T. pseudonana* and *T. oceanica* grown under 12:12 light–dark sinusoidal cycles with average daily photosynthetically available radiation about the same as the growth intensities used in our study (Vandennecke et al. 2015). The similarity in these growth rates (as well as many of the basic cell characteristics) under different light cycle regimes suggests that our application of continuous light is valid for evaluating photosynthetic energy use and applying the results to broader ecological settings, at least for these diatoms.

Chla decreased from 6.27 $\mu\text{g cell}^{-1}$ in the lowest light-acclimated cultures to 1.64 $\mu\text{g cell}^{-1}$ in the highest light-acclimated cultures. The decrease in cellular Chla with the increasing growth irradiance is a common characteristic of photoacclimation that was also reflected in the strong decrease in Chla:C with the increasing light-limited growth rate (Table 2). Constant C:N across growth rates confirmed that nitrogen was nonlimiting and was in agreement with previous studies on light-limited algae (Bartual and Gálvez 2002; Berges and Falkowski 1998; Sarthou et al. 2005). Thus, the behaviors reported here are attributable to physiological responses to light limitation.

The light dependence of cellular Chla:C was also reflected in the 12-fold decrease in Chla-specific NPP_C (NPP_C^b) between cells growing at 1.54 and 0.20 d^{-1} , mirroring the 12-fold decrease in growth irradiances (Table 2). However, the decrease in NPP_C^b with the decreasing light-limited growth rate was not associated with changes in

photosynthetic efficiency at PSII measured by F_v/F_M . F_v/F_M was maximal across all light-limited growth rates and was accompanied by only slight decreases in σ_{PSII} with the increasing growth irradiance (Table 2). The relative numbers of active PSII reaction centers (nPSII) were derived from the quotient of F_o and σ_{PSII} (Oxborough et al. 2012; Silsbe et al. 2015) and expressed normalized to Chl *a* and C for each light-limited growth rate (Table 2). nPSII Chl *a*⁻¹ did not change with light intensity, but nPSII C⁻¹ decreased with increasing light intensity. The \bar{a}^b values increased with irradiance from 0.0081 m² mg Chl *a*⁻¹ in the lowest light-limited cells to 0.0185 m² mg Chl *a*⁻¹ in cells acclimated to the highest light intensity, a result that was likely a consequence of higher photoprotective pigment content in cells growing at higher light intensities (MacIntyre et al. 2002).

PE curves were generated from measurements of GPP_{O₂}, NP_{O₂} and short-term (20 min) ¹⁴C-uptake. These data were normalized to Chl *a* (Fig. 1a–c) and cell carbon (Fig. 1d–f) to understand how photosynthetic energy is partitioned among the various metabolic demands of light-limited growth (Fig. 1). P_{max}^b from GPP_{O₂} and NP_{O₂/C} strongly increased, but α^b remained constant with light-limited growth rate (Fig. 1a, b; Table 3). These well-characterized behaviors in PE parameters caused E_k to shift strongly with growth irradiance (Table 3) and is, therefore, known as ‘ E_k -dependent variability’ (Behrenfeld et al. 2004). Maximum rates of Chl *a*-specific 20 min ¹⁴C-uptake also increased with light-limited growth rate, but both P_{max}^b and α^b determined from Chl *a*-specific ¹⁴C-uptake significantly increased with light-limited growth rate (Fig. 1c). Nevertheless, the parallel shifts in those PE parameters were insufficient to overcome growth rate-dependent changes in E_k (Table 3). Production at the growth irradiance (P_{ig}^b) was determined for each of the production metrics using the equations obtained by regression analysis. P_{ig}^b increased dramatically with growth rate in all three production metrics (Table 3). For cells grown at each light-limited growth rate, P_{ig}^b decreased from GPP_{O₂} to NP_{O₂/C} and to Chl *a*-specific ¹⁴C-uptake.

Cells grown at the lowest light-limited growth rate consistently showed higher α^C values when compared to cells grown at higher light-limited growth rates (Fig. 1d–f; Table 3). This result reflects the positive relationship between α^C and Chl *a*:C (MacIntyre et al. 2002). Carbon-specific PE data also provide a direct comparison to specific growth rate achieved for each light-limited culture. GPP_{O₂}^C will always overestimate specific growth rate because it is the sum of NPP_C and all of the energetic processes, including respiratory processes for ATP production, needed to fuel growth and division. However, because NP_{O₂/C}^C and ¹⁴C-uptake assess photosynthesis

Table 2 Light-limited cell characteristics in *T. pseudonana*

Growth rate (d ⁻¹)	Light intensity (μE)	Cells ml ⁻¹ (×10 ⁶)	Chl <i>a</i> (pg)	Chl <i>a</i> cell ⁻¹ (pg)	Chl <i>a</i> C ⁻¹ (×10 ⁻²) (μg μg ⁻¹)	C cell ⁻¹ (pg)	C:N	NPP (μmol C (mg Chl h) ⁻¹)	F_v/F_M	σ_{PSII}	\bar{a}^b (m ² (mg Chl a) ⁻¹)	nPSII (PSII Chl a ⁻¹) relative units	nPSII (PSII C ⁻¹) relative units
0.20	5	1.43 (0.14)	0.627 (0.065)	0.627 (0.065)	8.25 (0.57)	8.34 (0.66)	7.07 (0.49)	9 (1)	0.58 (0.00)	567 (8)	0.0081 (0.00005)	0.9 (0.3)	7.1 (0.3)
0.85	9	2.21 (0.37)	0.192 (0.020)	0.192 (0.020)	2.71 (0.20)	7.90 (0.49)	7.73 (0.37)	105 (10)	0.56 (0.02)	545 (26)	0.0169 (0.0012)	1.2 (0.2)	3.1 (0.2)
1.54	200	1.56 (0.05)	0.164 (0.008)	0.164 (0.008)	1.76 (0.21)	8.51 (0.19)	7.02 (0.23)	303 (25)	0.56 (0.03)	497 (5)	0.0185 (0.00009)	1.0 (0.1)	2.1 (0.1)

Values in parentheses represent SE for at least three independent continuous cultures

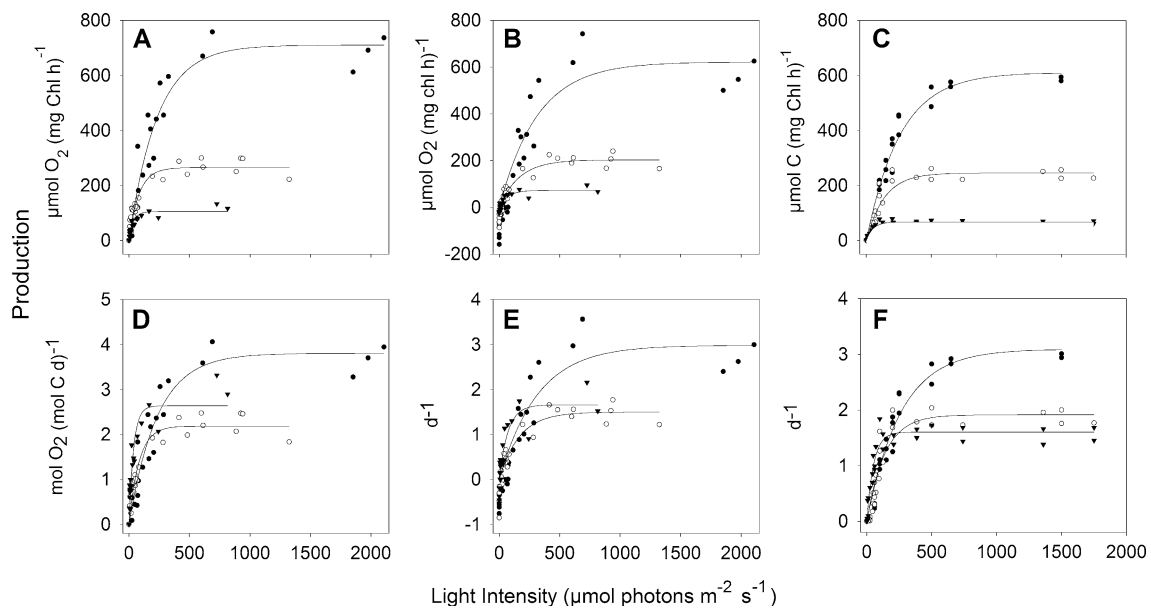


Fig. 1 PE relationships for light-limited *T. pseudonana* growing at 0.2 d⁻¹ (downward triangles), 0.85 d⁻¹ (open circles), and 1.5 d⁻¹ (filled circles) generated from measurements of GPP_{O₂}^b (a), NP_{O₂/C}^b (b), and Chla-specific 20 min ¹⁴C-uptake (c). PE relationships for

GPP_{O₂}^C (d), NP_{O₂/C}^C (e), and C-specific 20 min ¹⁴C-uptake (f) for cells growing at the same three light-limited growth rates

further downstream of the initial photosynthetic reactions, P_{Ig}^C for both NP_{O₂/C}^C and C-specific ¹⁴C-uptake provided reasonably good estimates of specific growth rate in light-limited cultures (Table 3).

Regardless of growth rate or the normalization factor (Chla or carbon) used in generating the PE relationships, α^b and α^C were always higher in GPP_{O₂}^b than NP_{O₂/C}^b or ¹⁴C-uptake determinations (Fig. 1). Finally, the maximum quantum efficiency (φ_m) determined from GPP_{O₂}^b was 0.10 mol O₂ (mol photons)⁻¹ in cells growing at 0.20 d⁻¹ and declined to 0.048 mol O₂ (mol photons)⁻¹ in cells growing at 1.54 d⁻¹ (Table 3). φ_m determined from NP_{O₂/C}^b similarly decreased 50 %, but φ_m determined from Chla-specific ¹⁴C-uptake decreased only 22 % between cells growing at the slowest and fastest light-limited growth rates (Table 3). Values of φ_m determined from NP_{O₂/C}^b and Chla-specific ¹⁴C-uptake were lower when compared to φ_m determined from GPP_{O₂}^b at each light-limited growth rate.

P_{Ig}^b determined from GPP_{O₂}^b and NPP_C^b for cells growing at each of the three light-limited growth rates strongly increased with light availability (Fig. 2a). These trends reversed when normalized to absorbed light using ā^b (Fig. 2a). The additional measurements of LDR^b, energy used for nitrate and sulfate reduction (DU_{NS}), and P_{Ig}^b from NP_{O₂/C}^b were used to evaluate how energy is allocated to major metabolic sinks across a wide range of light-limited growth rates. Whether normalized to Chla or absorbed

light, the dramatic changes in production with light-limited growth rate (Fig. 2a; Table 3) make it difficult to compare differences in energy allocation between growth rates. Therefore, all production values were normalized to GPP_{O₂}^b to show how photosynthetic energy was allocated to each of the major metabolic sinks across all growth rates (Fig. 2b).

Across all growth rates, the majority of energy derived through photosynthesis was retained in biomass carbon (Fig. 2, NPP_C, square symbols, green area). NPP_C:GPP_{O₂}^b was 0.57 in cells growing at the slowest growth rate and 0.70 in cells growing at the faster growth rates. In other words, 57 and 70 % of GPP_{O₂}^b were retained as organic carbon in cells growing at the slowest and fastest growth rates, respectively. A constant 5 % of GPP_{O₂}^b was used for reducing nitrate and sulfate (dark gray area) across all growth rates. The remaining energy derived from photosynthesis was allocated to oxygen and carbon consuming pathways that shifted in proportion depending on light-limited growth rate.

The fraction of GPP_{O₂}^b used for oxygen consumption pathways increased with the decreasing light-limited growth rates. LDR increased from 5 to 12 % of GPP_{O₂}^b with the decreasing growth rate (Fig. 2b, light gray area). Similarly, the fraction of GPP_{O₂}^b used for mitochondrial maintenance respiration (MMR; determined as the difference between GP_C and NP_{O₂/C}^b, Fig. 2b, yellow area) increased from 2 % in cells growing at 1.54 d⁻¹ to 8 % in cells growing at 0.20 d⁻¹. The same trend was found for

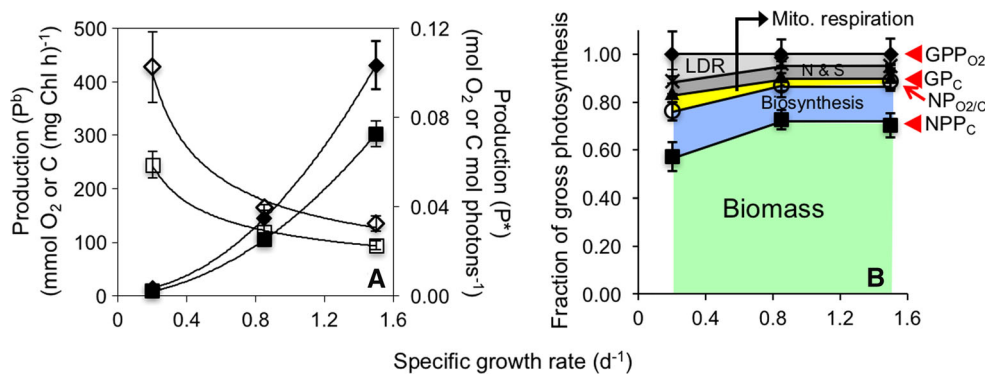


Fig. 2 **a** P_{Ig}^b for *T. pseudonana* growing at each of the three light-limited growth rates from GPP_{O₂}^b (filled diamonds) and NPP_C^b (filled squares) determined from cellular carbon. P_{Ig}^{*} values calculated using \bar{a}^b from GPP_{O₂}^{*} (open diamonds) and NPP_C^{*} determined from cellular carbon. **b** GPP_{O₂}^b (filled diamonds), GP_C^b (filled triangles), NP_{O₂/C}^b

(open circles), and NPP_C^b (filled squares) shown as fractions of GPP_{O₂}^b. Differences between these production measures are used to quantify energy allocated to LDR (light gray area), energy used for nitrate and sulfate reduction (dark gray area), MMR (yellow area), carbon catabolism for biosynthesis (blue area), and biomass (green area)

mitochondrial respiration rates measured in the dark (dark respiration, DR). However, DR was significantly greater than MMR in all cells regardless of the growth irradiance (Table 4). In contrast to energy allocated to respiratory pathways, the fraction of energy dedicated to carbon catabolism for biosynthesis (determined as the difference between NP_{O₂/C}^b and NPP_C^b) did not change between growth rates (Fig. 2, blue area).

Carbon excretion is another potential fate for photosynthetic energy. We measured DO¹⁴C accumulation in the filtrate of cultures incubated with NaH¹⁴CO₃ at their respective growth irradiances for 24 h. Across all growth rates, less than 2 % of GPP_{O₂}^b was lost as DO¹⁴C (data not shown). Although some DO¹⁴C could have been trapped on the filters, they were rinsed several times with media, and particulate organic carbon values determined from filters were never higher than cellular C determined by elemental analysis, suggesting that DO¹⁴C was not collected on filters.

Subcellular carbon allocation to different macromolecular pools varied dramatically depending on the time scale of the measurement. First, cells were incubated with NaH¹⁴CO₃ for 20 min (pulse labeling) to trace the fate of newly fixed carbon into carbohydrates, proteins, and lipid pools. In cells growing at the faster growth rates, the majority of newly fixed carbon was allocated to total carbohydrates and proteins (Fig. 3a). Very little newly fixed carbon was initially allocated to lipid biosynthesis in cells growing at any of the three light-limited growth rates (Fig. 3a). Regardless of growth rate, the aqueous alcohol fraction containing LMW metabolites was ≤3.0 % of the combined labeled macromolecular pools. Together, newly fixed carbohydrate, protein, and lipid pools matched gross carbon production (GP_C^b) in cells growing at 0.85 and

1.54 d⁻¹. In contrast, the sum of the three carbon pools was 3.3-fold less than GP_C^b in cells growing at 0.20 d⁻¹.

The macromolecular composition of the biomass of light-limited cells showed that the fraction of carbon allocated to biomass protein increased strongly with decreasing growth rate (Fig. 3b). Because the volume of culture needed to measure lipids was too large relative to the total culture volume, the amount of lipid in biomass was estimated by difference using the known cellular carbon values and the sum of total carbohydrate and protein fractions. This is likely an overestimation, but it provided an approximation of the amount of carbon allocated to the long-term lipid fraction. These carbon pools were also used to estimate the overall biochemical reduction state of the cells. The biomass carbon of cells growing at the slowest and middle growth rates was twofold to fourfold more reduced than newly fixed carbon, while the fastest growing cells maintained an equivalent biochemical reduction state despite changes in the relative concentrations of protein and lipids in newly fixed and long-term carbon (Table 5).

Discussion

Photosynthetic efficiencies and the various fates of photosynthetic energy were studied in *T. pseudonana* across a wide range of steady-state light-limited growth rates. A collection of oxygen and carbon production measurements, including GPP_{O₂}^b, LDR, NP_{O₂/C}^b, and NPP_C^b, together with information about pigment content and time-dependent changes in cellular carbon pools, were used to understand mechanisms diatoms use to tune their photosynthetic metabolism in response to light limitation. This collection of measurements facilitated photosynthetic energy assessments at various stages between, and including, the initial

Table 4 Light-dependent and mitochondrial respiration in light-limited *T. pseudonana*

Light-limited specific growth rate (d^{-1})	LDR, $\mu\text{mol O}_2$ (mg Chl h) $^{-1}$	<i>0.12</i>	Dark respiration (DR), $\mu\text{mol C}$ (mg Chl h) $^{-1}$	<i>1.12</i>	Maintenance mitochondrial respiration (MMR), $\mu\text{mol C}$ (mg Chl h) $^{-1}$	<i>0.076</i>
0.20	1.7 (0.4)	<i>0.12</i>	17.5 (4.3)	<i>1.12</i>	1.1	<i>0.076</i>
0.85	5.6 (1.8)	<i>0.04</i>	72.3 (16)	<i>0.50</i>	5.3	<i>0.039</i>
1.54	21.6 (3.0)	<i>0.05</i>	123 (36)	<i>0.29</i>	7.9	<i>0.018</i>

Values in parentheses for LDR, DR, and MMR represent SE for at least three independent cultures. The fraction of $\text{GPP}_{\text{O}_2}^{\text{b}}$ used for each of the respiratory processes is represented in italics

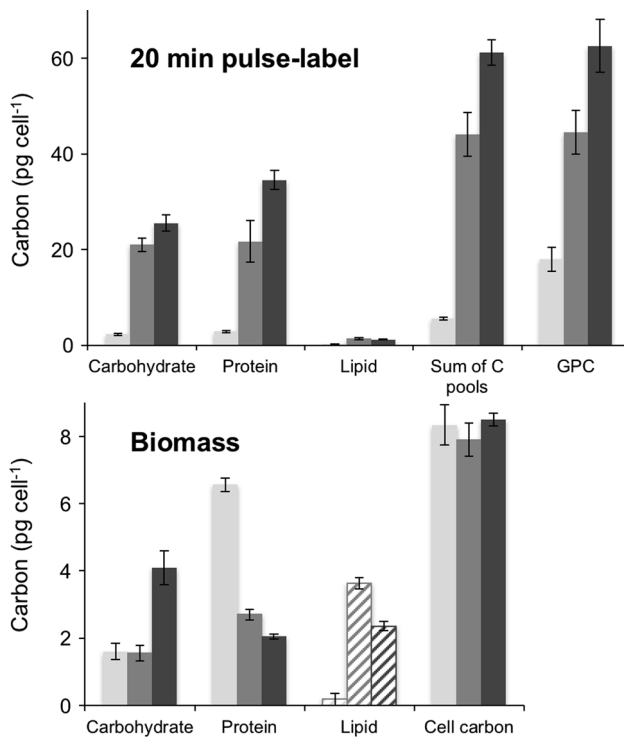


Fig. 3 Macromolecular composition of *T. pseudonana* growing at three light-limited growth rates: $0.2 d^{-1}$ (light gray bars), $0.85 d^{-1}$ (medium gray bars), $1.54 d^{-1}$ (dark gray bars) determined in cells pulse labeled for 20 min (top) and in biomass (bottom). Carbon content for carbohydrate, protein, and lipid were compared to bulk measures of GPC (top) and cell carbon (bottom). Biomass lipid pools (striped bars) were estimated

water-splitting, oxygen-producing reaction, and biomass production. Across all light-limited growth rates, *T. pseudonana* adjusts its photosynthetic machinery and cellular metabolism to maximize the efficiency of light energy conversion into biomass. Our results reveal new information about light-dependent shifts in photosynthetic energy allocation. These data support the idea that diatoms have unique growth rate-dependent energy use strategies that contribute to their global success. The data also illustrate other energy allocation strategies that are shared by diatoms and other microalgae and used to respond to growth

limitation. This work also shows that variability in PE parameters commonly used in productivity modeling is highly dependent on the metabolic measurement used to assess phytoplankton physiology.

Photoacclimation refers to fine-tuning of the light harvesting apparatus and downstream carbon metabolism to balance photosynthetic energy use in response to light availability. Several commonly observed characteristics of photoacclimation showed that our light-limited continuous cultures of *T. pseudonana* were fully acclimated to their light environments. For example, the constant F_v/F_M and strong increase in Chl*a*:C with the decreasing growth rate followed trends observed by others (Geider et al. 1997; Laws and Bannister 1980; Suggestt et al. 2009; Vandenhecke et al. 2015; Bittar et al. 2013). Although Chl*a*:C increased 4.75-fold between cells growing at 1.54 and $0.20 d^{-1}$, σ_{PSII} only increased slightly with the decreasing light-limited growth rate. Thus, as reflected in the relative changes in nPSII C^{-1} and nPSII Chl^{-1} (Table 2), cells increase numbers of PSII reaction centers and Chl*a* with the decreasing growth intensity to maintain maximal photosynthetic efficiency at low light-limited growth rate (Suggestt et al. 2009; Vandenhecke et al. 2015).

Behaviors in Chl*a*-normalized PE relationships that are characteristics of photoacclimation, namely constant α^{b} and variable $\text{P}_{\text{max}}^{\text{b}}$ causing major changes in E_k , were observed at the level of $\text{GPP}_{\text{O}_2}^{\text{b}}$ and $\text{NP}_{\text{O}_2}^{\text{b}}$ (Fig. 1a–c; Table 3). However, PE curves generated from Chl*a*-specific short-term ^{14}C -uptake rates showed α^{b} increased significantly with light-limited growth rate, albeit to a lesser extent than increases in $\text{P}_{\text{max}}^{\text{b}}$. Similar shifts in α^{b} generated from $\text{NP}_{\text{O}_2}^{\text{b}}$ were

Table 5 The biochemical reduction state of newly fixed and long-term cell carbon

Specific growth rate (d^{-1})	$\text{C}_r:\text{C}_o$	
	20 min	Biomass
0.20	2.6	4.2
0.85	1.1	4.1
1.54	1.4	1.1

$\text{C}_r:\text{C}_o$ is calculated as: (lipid + protein pools)/(carbohydrate pool)

observed in high and low-light-acclimated *T. weissflogii*, but the mechanism underlying that behavior was unknown (Post et al. 1985). Values of α^b generated from ^{14}C -uptake are influenced by the cellular lifetimes of newly fixed carbon, which are strongly influenced by metabolic demands that alter cellular energetic stoichiometry of ATP:NADPH (Halsey and Jones 2015). Investments of ATP into cell maintenance are highest at low growth rates (Kliphuis et al. 2012). To generate ATP for maintenance, slow growing *nutrient* limited cells rely heavily on rapid turnover of newly fixed carbon through glycolysis and mitochondrial respiration. Biosynthetic demand for NADPH is greater in fast-growing *nutrient*-limited cells and is primarily supplied through catabolism of longer-lived carbon storage forms that accumulate during the S phase of the cell cycle. Thus, the lifetimes of newly fixed carbon increase with *nutrient*-limited growth rate and during the S phase of the cell cycle (Halsey et al. 2013).

Growth rate-dependent differences in the lifetimes of newly fixed carbon were also shown in response to *light*-limited growth rate. The 20-min pulse labeling experiment showed the sum of the carbohydrate, protein, and lipid carbon pools matched GP_C in cells growing at the faster two growth rates but was only one-third of GP_C in cells growing at the slowest growth rate (Fig. 3). This result indicates that all of the carbon fixed during the 20 min incubation was retained in faster growing cells, but about two-thirds of the carbon fixed during the 20 min incubation was respired in slow growing cells (see also pulse labeling and biomass composition discussion below). Thus, the unexpected growth rate-dependent shifts in α^b derived from *Chla* specific 20 min ^{14}C -uptake measurements (Table 3; Fig. 1c) and from $\text{NP}_{\text{O}_2}^b$ in the Post et al.'s study demonstrate interpretation of PE relationships is complicated by growth rate-dependent changes in carbon metabolism during resource limitation.

PE measurements derived from physiological assessments of photosynthesis that are very close to the initial water-splitting reaction (i.e., $\text{GPP}_{\text{O}_2}^b$) yield α^b and α^c values that are significantly higher than values derived from measurements that assess photosynthetic energy further downstream because the energy harvested at PSII has not yet been consumed by other metabolic processes; such as respiration and carbon catabolism (Su et al. 2012). Variability in PE parameters also has important consequences when interpreting quantum yield determinations (ϕ_m). Shifts in α^b and α^c caused by growth rate-dependent carbon metabolism (see above) will also strongly affect ϕ_m because it is typically calculated by dividing α^b by \bar{a}^b . Using α^b generated from $\text{GPP}_{\text{O}_2}^b$ measurements, cells growing at 0.20 d^{-1} yielded a ϕ_m value of $0.101 \text{ mol O}_2 (\text{mol photons})^{-1}$, a value that is relatively close to the maximum theoretical quantum yield of 0.125 mol O_2

$(\text{mol photons})^{-1}$ and similar to the higher values generally found for diatoms (Langdon 1988). Because \bar{a}^b increases with growth rate, ϕ_m derived from $\text{GPP}_{\text{O}_2}^b$ was only 0.048 in cells growing at 1.54 d^{-1} . PE relationships generated from measurements that account for respiratory energy expenditures cause ϕ_m to be lower across all growth rates than relationships generated from measurements of GPP_{O_2} (Su et al. 2012). Thus, ϕ_m generated from $\text{NP}_{\text{O}_2/\text{C}}^b$ measurements were $0.084\text{--}0.042 \text{ mol C} (\text{mol photons})^{-1}$ and also decreased twofold from the slowest- to fastest-growing cells.

Finally, ϕ_m determined from ^{14}C -uptake PE relationships reflect the complicating influence of growth rate-dependent carbon catabolism. Importantly, the shifts in α^b driven by growth rate-dependent carbon metabolism offset the changes in \bar{a}^b that cause the characteristic growth rate-dependent changes in ϕ_m determined from $\text{GPP}_{\text{O}_2}^b$ and $\text{NP}_{\text{O}_2/\text{C}}^b$. These counteracting shifts in \bar{a}^b and α^b result in a significantly narrowed range of ϕ_m : $0.045\text{--}0.035 \text{ mol C} (\text{mol photons})^{-1}$ in cells growing at the slowest to fastest growth rates, respectively. Thus, interpretations of low ϕ_m values must take into account both the method used to assess photosynthetic physiology (i.e., the type of measurement that used to generate the PE curve) and growth rate-dependent metabolism.

Energy use efficiencies

Thalassiosira pseudonana is highly efficient at converting light energy to biomass under light-limiting conditions. Across all growth rates, $\text{NPP}_C^b:\text{GPP}_{\text{O}_2}^b$ was >0.50 , compared to values of ~ 0.33 where nitrogen was the limiting resource in diatoms and green algae (Halsey and Jones 2015; Jakob et al. 2007). A similarly high $\text{NPP}_C^b:\text{GPP}_{\text{O}_2}^b$ value was also measured in the diatom *Phaeodactylum tricornutum* when grown under light-limited conditions (Wagner et al. 2006). $\text{NPP}_C^b:\text{GPP}_{\text{O}_2}^b$ appears to be lower in phytoplankton from other taxonomic groups. $\text{NPP}_C^b:\text{GPP}_{\text{O}_2}^b$ was ~ 0.30 in a light-limited green alga and cyanobacterium (Wagner et al. 2006). Very low values (0.17) have been attributed to greater requirements for LDR processes (Kunath et al. 2012). Taken together, these data suggest that diatoms have evolved to be highly efficient at converting harvested light energy to biomass when light is the limiting resource. This high-energy-use efficiency may be a property that reflects diatom's adaptive life history.

Our results also suggest that energy use efficiencies vary depending on the limiting resource. Carefully controlled laboratory culture studies have revealed patterns of energy use that may be linked to adaptive physiology and growth conditions (Halsey and Jones 2015). For example, high $\text{NPP}_C^b:\text{GPP}_{\text{O}_2}^b$ values were also observed in a motile

prasinophyte, *Micromonas* sp. RCC299, and were attributed to physiological tradeoffs in energy investment strategies where high pigment content was maintained to achieve high photosynthetic rates even under very low nutrient availability (Halsey et al. 2014). More is needed to understand the combined effects of light and nitrogen limitation (Jakob et al. 2007). Nevertheless, these studies demonstrate a potential framework for predicting physiological responses and primary production under different environmental conditions given knowledge of the phytoplankton community.

Relationships between other measures of productivity are useful for understanding how photosynthetic energy is allocated to different metabolic pathways. For example, the difference between $\text{NPP}_{\text{O}_2/\text{C}}^{\text{b}}$ and $\text{NPP}_{\text{C}}^{\text{b}}$ quantifies energy used for biosynthesis of macromolecules that are more biochemically reduced than the initial product of carbon fixation, glyceraldehyde 3-phosphate (i.e., lipids, proteins). $\text{NPP}_{\text{C}}^{\text{b}}:\text{NPP}_{\text{O}_2/\text{C}}^{\text{b}}$ can be used to compare the magnitude of this metabolic sink across growth rates, between organisms, and in response to different environmental conditions. In this study, $\text{NPP}_{\text{C}}^{\text{b}}:\text{NPP}_{\text{O}_2/\text{C}}^{\text{b}}$ did not change across light-limited growth rates, a result that is consistent with an equivalent overall cellular carbon reduction state ($\text{C}_r:\text{C}_o$) in cells grown at 0.20 and 0.85 d^{-1} (Table 5). The much lower $\text{C}_r:\text{C}_o$ in cells grown at 1.54 d^{-1} was apparently driven by retention of carbohydrates (Fig. 3). These results were surprising because they are counter to our initial hypothesis that the need for more reductant (NADPH) for biosynthesis of energy-rich thylakoid membranes (i.e., lipids) at very low light-limited growth rates would dominate the $\text{NPP}_{\text{C}}^{\text{b}}:\text{NPP}_{\text{O}_2/\text{C}}^{\text{b}}$ relationship (Raven 1984). Instead, it appears that carbohydrate and protein content are the primary drivers of $\text{NPP}_{\text{C}}^{\text{b}}:\text{NPP}_{\text{O}_2/\text{C}}^{\text{b}}$. The $\text{NPP}_{\text{C}}^{\text{b}}:\text{NPP}_{\text{O}_2/\text{C}}^{\text{b}}$ value of ~ 0.77 in light-limited *T. pseudonana* is similar to $\text{NPP}_{\text{C}}^{\text{b}}:\text{NPP}_{\text{O}_2/\text{C}}^{\text{b}}$ values in light-limited *P. tricornutum* (Wagner et al. 2006). Lower ratios were observed in a cyanobacterium and a cryptophyte, respectively (Kunath et al. 2012), reflecting known species differences in the overall reduction state of biomass (Sukenic and Livne 1991).

Macromolecular composition

^{14}C -pulse labeling experiments together with measurements of biomass composition showed that the fate of newly fixed carbon differs depending on light-limited growth rate. In faster growing cells, the bulk of newly fixed carbon is allocated to longer-lived carbohydrates and proteins. Over the course of the cell cycle, carbohydrates are catabolized for two purposes: maintenance respiration and NADPH generation for biosynthesis of lipids and nucleic acids and other energy-rich molecules. We inferred from

cellular carbon quotas that lipid content was likely significantly greater in cells grown at 0.85 and 1.54 d^{-1} . However, LMW metabolites could constitute a significant fraction of biomass, causing us to overestimate lipid content. Cell lipid content estimated using an empirical thylakoid lipid mass value [kg per mol pigment from Raven (1984)] and measured Chl a content (Table 2), yielded only 0.34 pg lipid in the slowest-growing cells, supporting our conclusion that under very low light availability, cells retain very little energy in the lipid fraction of biomass compared to higher light-acclimated cells. These high-light cells are likely more heavily enriched in membrane phospholipids that are external to the chloroplast (Halsey et al. 2011). By far the largest fraction of photosynthate is ultimately retained in protein in the biomass of slowly growing light-limited cells, a result that was also found for nutrient-limited cultures (Halsey et al. 2011; Morris 1980).

Pathway gating between respiratory and other ATP producing pathways

Our set of photosynthetic measurements yielded rates for mitochondrial respiration in the dark (DR) and light (MMR) as well as short water–water cycles collectively referred to as light-dependent respiration (LDR). The relative contributions of these respiratory processes changed with light-limited growth rate. MMR determined at each growth irradiance in *T. pseudonana* (Fig. 2b, yellow area, $\text{GP}_{\text{C}}-\text{NP}_{\text{O}_2/\text{C}}$) was ~ 4 - to 14-fold lower than DR measured from oxygen loss rates in the dark during MIMS experiments (i.e., Fig. 1b or e, $\text{NP}_{\text{O}_2/\text{C}}$ production at zero light). This finding is consistent with previous studies that observed enhanced postillumination respiration, although the basis for the difference in DR and MMR is not understood (Bate et al. 1988; Geider et al. 1985; Weger et al. 1989). In *P. tricornutum*, DR was about ten times larger than MMR, but in that study, MMR did not change with growth intensity (Geider et al. 1985).

One explanation for the discrepancy in MMR and DR is that other respiratory processes, such as LDR, are upregulated in the light. The fraction of gross photosynthesis dedicated to LDR increased with the decreasing light-limited growth rates (Fig. 2b; Table 4). Thus LDR contributes to ATP production in the light and can help resolve at least some of the differences between DR and MMR. Furthermore, by switching to LDR pathways for ATP production in the light, cells reduce their reliance on catabolism of carbon stores for their total ATP requirements.

Another pathway that may supplement ATP production in the light is cyclic electron flow around PSI. This pathway has been implicated as an important metabolic process in high-light-acclimated and unstressed diatoms (Fietz and Nicklisch

2002; Thamtrakoln et al. 2013; Wagner et al. 2006). However, because it contributes neither to O₂ nor carbon flux, we could not capture the contribution of cyclic PSI transport to the overall photosynthetic energy budget in light-limited *T. pseudonana* using our collection of measurements.

Our results suggest that pathway gating between LDR and/or cyclic PSI transport and MMR is especially important for cells such as diatoms with life histories that include deep mixing. A primary difference between the former two pathways (LDR and cyclic PSI transport) and MMR is the source of electrons used to drive ATP synthesis. For MMR, carbon oxidation produces NADH that is fed into the respiratory electron transport chain. In contrast, LDR can occur prior to carbon fixation by reduction of O₂ to H₂O on the stromal side of the thylakoid membrane to enhance the proton motive force for ATP generation (Asada 1999). LDR includes the malate valve that shuttles reductant from the plastid to the mitochondrial respiratory electron transport chain, possibly employing an alternative oxidase (AOX) (Allen et al. 2008). Reductant shuttling to AOX was recently shown to be an important ATP generating process in diatoms (Prihoda et al. 2012; Bailleul et al. 2015).

The sensitivity of LDR, and possibly cyclic PSI transport, to light-limited growth rate suggests that these pathways are highly tuned to light availability, and they supplement ATP production derived from MMR. Cyclic electron transport around PSI bypasses transfer of electrons to NADPH via ferredoxin and, instead, returns electrons to the Q-pool within the photosynthetic electron transport chain, thus promoting the proton motive force to generate ATP. Switching from 100 % DR in the dark to ~50 % MMR plus ~50 % LDR/cyclic PSI transport in the light, when averaged among all light-limited growth rates, is a form of pathway gating that we suggest is important to conserve carbon stores when light availability is scarce.

Diatoms are dominant members of the phytoplankton community during seasonal deep mixing events and in turbulent coastal regions. Our results suggest that pathway gating of electrons and carbon in response to light availability is an important mechanism that underlies high growth efficiencies in diatoms during low light conditions. This study supports the idea that the unique compartmental organization of proteins involved in carbon metabolism in diatoms (Smith et al. 2012; Wilhelm et al. 2006) may be especially important in regulating the flux of carbon and energy depending on light availability.

Conclusions

- (1) *Thalassiosira pseudonana* is extremely efficient at converting harvested light energy into biomass. Across all growth rates, more than 57 % of harvested

light energy was retained as biomass. The majority of carbon biomass was retained in the protein fraction in the slowest-growing cells, while lipids and carbohydrates were more prevalent in faster growing cells. The carbon composition of fast and slow growing light-limited cells reflects the metabolic demands for different ratios of the energetic currencies, ATP, and NADPH. At low growth rates, requirements for maintenance energy in the form of ATP dominate and are fulfilled through MMR strongly supplemented by alternative pathways for ATP production, including LDR.

- (2) The well-known influences of photoacclimation on Chl_a-normalized PE behaviors, namely constant α^b and the increasing P_{max}^b with the increasing growth rate, are not observed in PE curves generated from short-term Chl_a-specific ¹⁴C-uptake measurements. The influences of growth rate-dependent carbon metabolism cause α^b to increase with growth rate, and cause ϕ_m to be significantly constrained compared to ϕ_m derived from $GPP_{O_2}^b$. Energetic expenditures (e.g., LDR, mitochondrial respiration) cause ϕ_m to decrease as energy assessments are made further downstream of PSII.
- (3) Diatoms shift between ATP generating pathways to achieve high growth efficiencies at low light. At low light intensities, LDR contributes a greater proportion of ATP production than MMR. The enhanced role of LDR (and possibly cyclic PSI transport) at low light-limited growth rates may function to conserve carbon stores, which would be depleted by MMR. Pathway gating between different respiratory pathways and other alternative pathways for ATP generation appears to balance the cells' needs for ATP and carbon storage.

In this study, we have discovered that diatoms achieve a high efficiency of light energy conversion to biomass at low light levels by redistributing energy to more efficient ATP generating pathways. The evidence presented here reveals in more detail how diatoms succeed by controlling their metabolism. The challenge ahead is to determine whether other microalgae use similar mechanisms or have different adaptive properties of photosynthetic metabolism. Moreover, because of the role played by 'omics in modern plankton ecology, it will be important to understand the specific molecular mechanisms that implement this adaptive control and to compare across genomes to understand their origin and distribution across diverse phytoplankton taxa.

Acknowledgments The authors thank Dr. Douglas Campbell and an anonymous reviewer for their careful reading and comments and suggestions that significantly improved the final manuscript. We also

thank Greg Silsbe for helpful discussions during the final stages of manuscript preparation. This work was funded by a grant from the National Science Foundation Biological Oceanography program (NSF-OCE 1057244).

References

- Allen JF (2003) Cyclic, pseudocyclic and noncyclic photophosphorylation: new links in the chain. *Trends Plant Sci* 8(1):15–19
- Allen AE, La Roche J, Maheswari U, Lommer M, Schauer N, Lopez PJ, Finazzi G, Fernie AR, Bowler C (2008) Whole-cell response of the pennate diatom *Phaeodactylum tricornutum* to iron starvation. *Proc Natl Acad Sci* 105(30):10438–10443
- Asada K (1999) The water-water cycle in chloroplasts: scavenging of active oxygens and dissipation of excess photons. *Annu Rev Plant Physiol Plant Mol Biol* 50:601–639
- Bailleul B, Berne N, Murik O, Petroustos D, Pihoda J, Tanaka A, Villanova V, Bigny R, Flori S, Falconet D, Drieger-Liszkay A, Santabarbara S, Rappaport F, Joliot P, Tirichine L, Falkowski P, Cardol P, Bowler C, Finazzi G (2015) Energetic coupling between plastids and mitochondria drives CO₂ assimilation in diatoms. *Nature* 524:366–369
- Bartual A, Gálvez JA (2002) Growth and biochemical composition of the diatom *Phaeodactylum tricornutum* at different pH and inorganic carbon levels under saturating and subsaturating light regimes. *Bot Mar* 45(6):491–501
- Bate GC, Sueltemeyer DF, Fock HP (1988) ¹⁶O₂/¹⁸O₂ analysis of oxygen exchange in *Dunaliella tertiolecta*. Evidence for the inhibition of mitochondrial respiration in the light. *Photosynth Res* 16:219–231
- Behrenfeld MJ, Prasil O, Babin M, Bruyant F (2004) In search of a physiological basis for covariations in light-limited and light-saturated photosynthesis. *J Phycol* 40:4–25
- Behrenfeld MJ, Halsey KH, Milligan AJ (2008) Evolved physiological responses of phytoplankton to their integrated growth environment. *Philos Trans R Soc Lond B* 363(1504):2687–2703
- Berges JA, Falkowski PG (1998) Physiological stress and cell death in marine phytoplankton: induction response to nitrogen or light limitation. *Limnol Oceanogr* 43(1):129–135
- Bittar TB, Lin Y, Sassano LR, Wheeler BJ (2013) Carbon allocation under light and nitrogen resource gradients in two model marine phytoplankton. *J Phycol* 49:523–535
- Bowler C, De Martino A, Falciatore A (2010) Diatom cell division in an environmental context. *Curr Opin Plant Biol* 13:623–6630
- Crombet Y, Leblanc K, Quéguiner B, Moutin T, Rimmelin P, Ras J, Claustre H, Leblond N, Orío L, Pujo-Pay M (2011) Deep silicon maxima in the stratified oligotrophic Mediterranean Sea. *Biogeosciences* 8:459–475
- Dubinsky Z, Falkowski PG, Post AF, van Hes UM (1987) A system for measuring phytoplankton photosynthesis in a defined light field with an oxygen electrode. *J Plankton Res* 9:607–612
- Field CB, Behrenfeld MJ, Randerson JT, Falkowski P (1998) Primary production of the biosphere: integrating terrestrial and oceanic components. *Science* 281(5374):237–240
- Fietz S, Nicklisch A (2002) Acclimation of the diatom *Stephanodiscus neoastraea* and the cyanobacterium *Planktothrix agardhii* to simulated natural light fluctuations. *Photosynth Res* 72:95–106
- Flynn KJ (2001) A mechanistic model for describing dynamic multi-nutrient, light, temperature interactions in phytoplankton. *J Plankton Res* 23(9):977–997
- Furnas MJ (1990) In situ growth rates of marine phytoplankton: approaches to measurement, community and species growth rate. *J Plankton Res* 12:1117–1151
- Geider RJ (1987) Light and temperature dependence of the carbon to chlorophyll ratio in microalgae and cyanobacteria: implications for physiology and growth of phytoplankton. *New Phytol* 106:1–34
- Geider RJ, Osborne BA, Raven JA (1985) Light dependence of growth and photosynthesis in *Phaeodactylum tricornutum* (Bacillariophyceae). *J Phycol* 21:609–619
- Geider RJ, MacIntyre HL, Kana TM (1997) Dynamic model of phytoplankton growth and acclimation: responses of the balanced growth rate and the chlorophyll a:carbon ratio to light, nutrient-limitation and temperature. *Mar Ecol Prog Ser* 148(1–3):187–200
- Geider RJ, MacIntyre HL, Kana TM (1998) A dynamic regulatory model of phytoplankton acclimation to light, nutrients, and temperature. *Limnol Oceanogr* 43(4):679–694
- Geider RJ, Moore CM, Ross ON (2009) The role of cost-benefit analysis in models of phytoplankton growth and acclimation. *Plant Ecol Divers* 2(2):165–178
- Granum E, Kirkvold S, Mykkestad SM (2002) Cellular and extracellular production of carbohydrates and amino acids by the marine diatom *Skeletonema costatum*: diel variations and effects of N depletion. *Mar Ecol Prog Ser* 242:83–94
- Guillard RRL (1975) Culture of phytoplankton for feeding marine invertebrates. In: Smith WL, Chanley MH (eds) Culture of marine invertebrate animals. Plenum Press, New York, pp 26–60
- Halsey KH, Jones BM (2015) Phytoplankton strategies for photosynthetic energy allocation. *Annu Rev Mar Sci* 7:265–297
- Halsey KH, Milligan AJ, Behrenfeld MJ (2010) Physiological optimization underlies growth rate-independent chlorophyll-specific gross and net primary production. *Photosynth Res* 103(2):125–137
- Halsey KH, Milligan AJ, Behrenfeld MJ (2011) Linking time-dependent carbon-fixation efficiencies in *Dunaliella tertiolecta* (Chlorophyceae) to underlying metabolic pathways. *J Phycol* 47(1):66–76
- Halsey KH, O'Malley RT, Graff JR, Milligan AJ, Behrenfeld MJ (2013) A common partitioning strategy for photosynthetic products in evolutionarily distinct phytoplankton species. *New Phytol* 198(4):1030–1038
- Halsey KH, Milligan AJ, Behrenfeld MJ (2014) Contrasting strategies of photosynthetic energy utilization drive lifestyle strategies in ecologically important picoeukaryotes. *Metabolites* 4:260–280
- Ho T-Y, Quigg AS, Finkel ZV, Milligan AJ, Wyman K, Falkowski PG, Morel FMM (2003) The elemental composition of some marine phytoplankton. *J Phycol* 39:1145–1159
- Jakob T, Wagner H, Stehfest K, Wilhelm C (2007) A complete energy balance from photons to new biomass reveals a light- and nutrient-dependent variability in the metabolic costs of carbon assimilation. *J Exp Bot* 58(8):2101–2112
- Kliphuis AMJ, Klok AJ, Martens DE, Lamers PP, Janssen M, Wijffels RH (2012) Metabolic modeling of *Chlamydomonas reinhardtii*: energy requirements for photoautotrophic growth and maintenance. *J Appl Phycol* 24(2):253–266
- Kolber Z, Prasil O, Falkowski PG (1998) Measurements of variable fluorescence using fast repetition rate techniques: defining methodology and experimental protocols. *Biochim Biophys Acta* 1367:88–106
- Kooistra WHCF, Medlin LK (2007) Species concepts in diatoms: a clarification. *Diatom Res* 22:227–228
- Kunath C, Jakob T, Wilhelm C (2012) Different phycobilin antenna organisations affect the balance between light use and growth rate in the cyanobacterium *Microcystis aeruginosa* and in the cryptophyte *Cryptomonas ovata*. *Photosynth Res* 111(1–2):173–183

- Langdon C (1988) On the causes of interspecific differences in the growth-irradiance relationship for phytoplankton. *J Plankton Res* 37:715–730
- Laws EA, Bannister TT (1980) Nutrient- and light-limited growth of *Thalassiosira fluviatilis* in continuous culture, with implications for phytoplankton growth in the ocean. *Limnol Oceanogr* 25(3):457–473
- MacIntyre HL, Cullen JJ (2005) Using cultures to investigate the physiological ecology of microalgae. In: Andersen RA (ed) *Algal culturing techniques*. Elsevier, Amsterdam, pp 287–326
- MacIntyre HL, Kana TM, Anning T, Geider RJ (2002) Photoacclimation of photosynthesis irradiance response curves and photosynthetic pigments in microalgae and cyanobacteria. *J Phycol* 38:17–38
- Margalef R (1978) Life-forms of phytoplankton as survival alternatives in an unstable environment. *Oceanol Acta* 1:493–509
- Mitchell BG, Kahru M, Wieland J, Stramska M (2003) Determination of spectral absorption coefficients of particles, dissolved material and phytoplankton for discrete water samples. In: Mueller JL, Fargoin GS, McClain CR (eds) *Ocean optics protocols for satellite ocean color sensor validation, revision 4, vol 4*. NASA/TM-2003, Greenbelt
- Morris I (1980) Paths of carbon assimilation in marine phytoplankton. In: Falkowski PG (ed) *Primary productivity in the sea*. Plenum Press, New York, pp 139–159
- Oxborough K, Moore CM, Suggett D, Lawson T, Chan HG, Geider RJ (2012) Direct estimation of functional PSII reaction center concentration and PSII electron flux on a volume basis: a new approach to the analysis of Fast Repetition Rate fluorometry (FRRf) data. *Limnol Oceanogr Methods* 10(3):142–154
- Post AF, Dubinsky Z, Wyman K, Falkowski PG (1985) Physiological responses of a marine planktonic diatom to transitions in growth irradiance. *Mar Ecol Prog Ser* 25:141–149
- Prihoda J, Tanaka A, de Paula WBM, Allen JF, Tirichine L, Bowler C (2012) Chloroplast-mitochondria cross-talk in diatoms. *J Exp Bot* 63(4):1543–1557
- Raven JA (1984) A cost-benefit analysis of photon absorption by photosynthetic unicells. *New Phytol* 98:593–625
- Ritchie RJ (2006) Consistent sets of spectrophotometric chlorophyll equations for acetone, methanol and ethanol solvents. *Photosynth Res* 89:27–41
- Sarthou G, Timmermans KR, Blain S, Tréguer P (2005) Growth physiology and fate of diatoms in the ocean: a review. *J Sea Res* 53:25–42
- Silsbe GM, Oxborough K, Suggett DJ, Forster RM, Ihnken S, Komárek O, Lawrenz E, Prášil O, Röttgers R, Šicner M, Simis S, Van Dijk MA, Kromkamp JC (2015) Toward autonomous measurements of photosynthetic electron transport rates: an evaluation of active fluorescence-based measurements of photochemistry. *Limnol Oceanogr Methods* 13:138–155
- Singh D, Carlson R, Fell D, Poolman M (2015) Modelling metabolism of the diatom *Phaeodactylum tricornutum*. *Biochem Soc Trans* 43(6):1182–1186
- Six C, Finkel ZV, Rodriguez F, Marie D, Partensky F, Campbell DA (2008) Contrasting photoacclimation costs in ecotypes of the marine eukaryotic picoplankton *Ostreococcus*. *Limnol Oceanogr* 53(1):255–265
- Smetacek V (1999) Diatoms and the ocean carbon cycle. *Protist* 150:25–32
- Smith REH, Geider RJ (1985) Kinetics of intracellular carbon allocation in a marine diatom. *J Exp Mar Biol Ecol* 93:191–210
- Smith REH, Platt T (1984) Carbon exchange and ¹⁴C tracer methods in a nitrogen-limited diatom *Thalassiosira pseudonana*. *Mar Ecol Prog Ser* 16(1–2):75–87
- Smith SR, Abbriano RM, Hildebrand M (2012) Comparative analysis of diatom genomes reveals substantial differences in the organization of carbon partitioning pathways. *Algal Res* 1(1):2–16
- Su W, Jakob T, Wilhelm C (2012) The impact of nonphotochemical quenching of fluorescence on the photon balance in diatoms under dynamic light conditions. *J Phycol* 48:336–346
- Suggett DJ, Moore CM, Hickman AE, Geider RJ (2009) Interpretation of fast repetition rate (FRR) fluorescence: signatures of phytoplankton community structure versus physiological state. *Mar Ecol Prog Ser* 376:1–19
- Sukenik A, Livne A (1991) Variations in lipid and fatty-acid content in relation to acetyl CoA carboxylase in the marine prymnesiophyte *Isochrysis-galbana*. *Plant Cell Physiol* 32(3):371–378
- Thamatrakoln K, Bailleul B, Brown CM, Gorbunov MY, Kustka AB, Frada M, Joliot PA, Falkowski PG, Bidle KD (2013) Death-specific protein in a marine diatom regulates photosynthetic responses to iron and light availability. *Proc Natl Acad Sci* 110(50):20123–20128
- Vandennecke JMR, Bastedo J, Cockshutt AM, Campbell DA, Huot Y (2015) Changes in the Rubisco to photosystem ratio dominate photoacclimation across phytoplankton taxa. *Photosynth Res* 124(3):275–291
- Wagner H, Jakob T, Wilhelm C (2006) Balancing the energy flow from captured light to biomass under fluctuating light conditions. *New Phytol* 169:95–108
- Weger HG, Herzig R, Falkowski PG, Turpin DH (1989) Respiratory losses in the light in a marine diatom: measurements by short-term mass spectrometry. *Limnol Oceanogr* 34(7):1153–1161
- Wilhelm C, Buchel C, Fisahn J, Goss R, Jakob T, LaRoche J, Lavaud J, Lohr M, Riebesell U, Stehfest K, Valentin K, Kroth PG (2006) The regulation of carbon and nutrient assimilation in diatoms is significantly different from green algae. *Protist* 157:91–124